# Reactions of Metal-Cluster Carbonyls in Pillared Clay Galleries: Surface Coordination Chemistry and Fischer-Tropsch Catalysis

**Emmanuel P. Giannelis, Edward G. Rightor, and Thomas J. Pinnavaia***

*Contribution from the Department of Chemistry and Center for Fundamental Materials Research, Michigan State University, East Lansing, Michigan 48824.*
*Received September 21, 1987*

**Abstract:** The surface chemistry of metal-cluster carbonyl complexes $M_3(CO)_{12}$ (M = Ru, Os), $Ir_4(CO)_{12}$, $H_2Os_3(CO)_{12}$, and $H_4Ru_4(CO)_{12}$ encapsulated in the galleries (interlayers) of an alumina pillared montmorillonite (APM) has been investigated by infrared spectroscopy. The trinuclear complexes in $CH_2Cl_2$ solution bind as protonated $HM_3(CO)_{12}^+$ cations, a reaction that illustrates the exceptional Brønsted acidity of the gallery surfaces even at ambient temperatures, In the presence of excess physisorbed water, the gallery acidity is reduced, and the clusters bind through physical adsorption as neutral $M_3(CO)_{12}$ complexes. The more weakly basic $Ir_4(CO)_{12}$ cluster binds by physical adsorption, regardless of water content. After they were aged at 25 °C or heated to 110–150 °C, the gallery-bound tri- and tetranuclear clusters react with hydroxyl groups on the alumina pillar to form pillar-grafted, mononuclear ensembles of the type $[M(CO)_x(OAl{\equiv})_2]_n$ with $n = 2, 3$. The reactions of $H_2Os_3(CO)_{12}$ and $H_4Ru_4(CO)_{12}$ with APM afford the same type of grafted complexes, except that $H_2Os_3(CO)_{12}$ also forms a grafted $HOs_3(CO)_{10}(OAl{\equiv})$ cluster as a gallery intermediate. These grafting reactions parallel those observed on the surfaces of bulk alumina. The reduction of $[HRu_3(CO)_{12}^+]$–APM in hydrogen affords crystalline ruthenium aggregates (<50 Å) embedded within the clay particles. As a catalyst for Fischer–Tropsch (FT) hydrocarbon synthesis, the Ru–APM exhibits unusual selectivity toward branched products. Chain branching is attributed to the surface rearrangements of carbonium ions formed by the protonation of FT terminal olefins. Thus, a novel dual functionality is demonstrated for the metal oxide pillared clay. The pillars mimic a bulk oxide surface by providing functional hydroxyl groups for metal immobilization, while the galleries afford zeolitic microporosity and acidity for catalytic selectivity.

Pillared clays are a new family of microporous solids formed by the intercalation of robust cations in the galleries (interlayers) of smectites and related 2:1 layered silicate structure types.[1-7] By adjusting the size of the pillaring cations and the separation between them, one can vary the pore size distribution over a broad range and thereby design microporous environments different from those afforded by conventional three-dimensional zeolites. Thus, pillared clays provide a new kind of intracrystalline arena for shape-selective adsorption and catalysis,

Clays interlayered with polyoxo cations are important precursors to pillared metal oxide derivatives with selective Brønsted and Lewis acid catalytic properties. For instance, alumina[1,2] and zirconia[1,7] pillared clays, formed by the calcination of intercalates containing the corresponding polyoxometal ions,[1-3,7] are highly selective catalysts for the cracking of petroleum,[8-10] the dehydration of alcohols,[11,12] and a variety of other acid-catalyzed reactions.[13-15] Alternative synthetic strategies are being explored to broaden the catalytic versatility of pillared clays by introducing more active transition-metal elements in the gallery environment, New polyoxo cation pillaring agents containing chromium,[16,17] iron,[18] and titanium[19] have added to the pillared clay family and have opened the door to possible applications in electron-transfer catalysis, In addition, clays interlayered with metal-cluster complexes, such as those containing $M_6X_{12}^{n+}$ (M = Nb, Ta; $n$ = 2–4) and $M_6X_8^{n+}$ (M = Mo; $n = 4$) cores, have been converted to metal oxide pillared forms with potential utility for oxidation catalysis,[20,21]

All of these previous approaches to pillared clays have relied on the existence of polynuclear cations suitable for intercalation and subsequent transformation to stable metal oxide aggregates. However, not all catalytically interesting transition elements form polynuclear cations appropriate for exchange into clays. A potentially more versatile approach would be to introduce transition-metal centers into clays that already have been pillared with a thermally stable oxide (e.g., alumina or zirconia). Conventional impregnation methods have been initiated recently to achieve metal dispersions on pillared clays,[22] but such techniques generally lack the specificity offered by molecular pathways.

The present work reports a new method for introducing transition-metal centers in the galleries of a thermally stable pillared clay. Our approach focuses on the reactions of metal-cluster carbonyl complexes with protons and surface hydroxyl groups of an alumina pillared montmorillonite, henceforth abbreviated APM. The surface chemistry of tri- and tetranuclear ruthenium, osmium, and iridium carbonyls is examined in comparison to the chemistry of these species on the surfaces of bulk oxides.[23-30] Also, we report

(1) Vaughan, D. E. W.; Lussier, R. J. Preprints of the 5th International Conference on Zeolites, Naples, Italy, June 2–6, 1980.
(2) Pinnavaia, T. J. *Science (Washington, D.C.)* **1983**, *220*, 365.
(3) Lahav, N.; Shani, U.; Shabtai, J. *Clays Clay Miner.* **1978**, *26*, 107.
(4) Barrer, R. M. *Zeolites and Clay Minerals as Sorbents and Molecular Sieves*; Academic: New York, 1978.
(5) Shabtai, J. *Chim. Ind. (Milan)* **1979**, *61*, 734.
(6) Loeppert, R. H., Jr.; Mortland, M. M.; Pinnavaia, T. J. *Clays Clay Miner.* **1979**, *27*, 201.
(7) Yamanaka, S.; Brindley, G. W. *Clays Clay Miner.* **1979**, *27*, 119
(8) Shabtai, J.; Lazar, R.; Oblad, A. G. *Stud. Surf. Sci. Catal.* **1981**, *7*, 828.
(9) Lussier, R. J.; Magee, J. S.; Vaughan, D. E. W. Preprints of the 7th Canadian Synposium on Catalysis; Edmonton, Alberta, Canada, Oct 19–22, 1980.
(10) Occelli, M. L. *Ind. Eng. Chem. Prod. Res. Dev.* **1983**, *22*, 553.
(11) Occelli, M. L.; Innes, R. A.; Hwu, F. S. S.; Hightower, J. W. *Appl. Catal.* **1985**, *14*, 69.
(12) Burch, R.; Warburton, C. I. *J. Catal.* **1986**, *97*, 511.
(13) Occelli, M.; Hsu, J. T.; Galya, L. G. *J. Mol. Catal.* **1985**, *33*, 371.
(14) Kibuchi, E.; Matsuda, T.; Ueda, J.; Morita, Y. *Appl. Catal.* **1985**, *16*, 401.
(15) Ballantine, J. A. In *Chemical Reactions in Organic and Inorganic Constrained Systems*; Setton, R., Ed.; Reidel: New York, 1986; pp 197–212.
(16) Pinnavaia, T. J.; Tzou, M. S.; Landau, S. D. *J. Am. Chem. Soc.* **1985**, *107*, 2783.
(17) Carrado, K. A.; Suib, S. L.; Skoularikis, N. D.; Coughlin, R. W. *Inorg. Chem.* **1986**, *25*, 4217.
(18) Yamanaka, S.; Doc, T.; Sako, S.; Hattori, M. *Mater. Res. Bull.* **1984**, *19*, 161.
(19) Sterte, J. *Clays Clay Miner.* **1986**, *34*, 658.
(20) Christiano, S. P.; Wang, J.; Pinnavaia, T. J. *Inorg. Chem.* **1985**, *24*, 1222.
(21) Christiano, S. P.; Pinnavaia, T. J. *J. Solid State Chem.* **1986**, *64*, 232.
(22) Parulekar, V. N.; Hightower, J. W. *Appl. Catal.*, in press.
(23) Knözinger, H.; Zhao, Y. *J. Catal.* **1981**, *71*, 337.
(24) Deeba, M.; Gates, B. C. *J. Catal.* **1981**, *67*, 303.
(25) Psaro, R.; Ugo, R.; Zanderighi, G. M.; Besson, B.; Smith, A. K.; Bassett, J. M. *J. Organomet. Chem.* **1981**, *13*, 215.
(26) Crawford, J. E.; Melson, G. A.; Makovsky, L. E.; Brown, F. R. *J. Catal.* **1983**, *83*, 454.
(27) Kuznetsov, V. L.; Bell, A. T.; Yermakov, Y. I. *J. Catal.* **1980**, *65*, 374.
(28) Theolier, A.; Choplin, A.; D'Ornelas, L.; Basset, J. M.; Zanderighi, G. M.; Ugo, R.; Psaro, R.; Sourisseau, C. *Polyhedron* **1983**, *2*, 119.

0002-7863/88/1510-3880$01.50/0 

Table I. Carbonyl-Stretching Frequencies[a]

| compound | $\nu$(CO), cm$^{-1}$ |
|---|---|
| $[HOs_3(CO)_{12}^+]$–APM | 2134 s, 2100 s, 2074 vs, 2061 s, 2023 m |
| $[HOs_3(CO)_{12}^+][PF_6]$ | 2134 s, 2101 s, 2077 vs, 2058 s, 2018 m |
| $[Os_3CO_{12}]$–APM | 2068 s, 2034 s, 2014 m, 2001 m |
| $Os_3CO_{12}$ | 2068 vs, 2034 s, 2013 m, 2000 m |
| $[Os(CO)_x(OAl\equiv)_2]_n$–APM | 2032 s, 2045 vs, 1978 m |
| $[HRu_3(CO)_{12}^+]$–APM | 2128 s, 2099 s, 2077 vs, 2060 s, 2030 s |
| $[HRu_3(CO)_{12}^+][PF_6^-]$ | 2128 s, 2100 s, 2077 vs, 2062 s, 2025 m |
| $[Ru_3(CO)_{12}]$–APM | 2060 vs, 2029 s, 2010 m |
| $Ru_3(CO)_{12}$ | 2061 vs, 2029 s, 2011 m |
| $[Ir_4(CO)_{12}]$–APM | 2109 w, 2060 vs, 2026 s |
| $Ir_4(CO)_{12}$ | 2112 w, 2059 vs, 2020 s |
| $[Ir(CO)_2(OAl\equiv)]_n$–APM | 2061 s, 1988 m |
| $[HOs_3(CO)_{10}(OAl\equiv)]$–APM | 2101 m, 2068 vs, 2056 vs, 2019 s, 2005 m |
| $[H_4Ru_4(CO)_{12}]$–APM2 | 2081 s, 2066 vs, 2024, 2005 sh |
| $H_4Ru_4(CO)_{12}$ | 2081 s, 2066 vs, 2024 s, 2009 sh |

[a] All carbonyl-stretching frequencies were recorded with mull samples, except for $Os_3(CO)_{12}$, $Ru_3(CO)_{12}$, and $H_4Ru_4(CO)_{12}$, which were observed with $CH_2Cl_2$ solutions.

the formation of supported ruthenium aggregates in the intracrystalline environment of the clay and describe the Fischer–Tropsch (FT) product selectivity of this new catalyst system.

## Experimental Section

**Materials.** Alumina pillared montmorillonite was prepared according to a previously described method[31] by the reaction of sodium montmorillonite (Crook County, WY) with an aluminum chlorohydrate solution (Chlorhydrol, Reheis Chemical Co.) containing $Al_{13}O_4(OH)_{24}(H_2O)_{12}^{7+}$ cations. The product was air-dried, heated under vacuum at 350 °C for 2 h, and allowed to cool in air. The $N_2$ BET surface area after outgassing under vacuum at 350 °C was 300 m$^2$/g. Chemical analysis by plasma emission spectroscopy indicated the unit cell composition to be as follows:

$$[Al(OH)_{2.80}]_{2.87}[Al_{3.11}Fe_{0.42}Mg_{0.48}]_{4.01}(Si_{7.92}Al_{0.08})O_{20}(OH)_4$$

The metal-cluster carbonyls $Os_3(CO)_{12}$, $Ru_3(CO)_{12}$, $H_4Ru_4(CO)_{12}$, and $Ir_4(CO)_{12}$ were purchased from Strem Chemicals, Inc. $H_2Os_3(CO)_{12}$ was prepared according to the method of Kaesz and co-workers.[32] All solvents were reagent grade and were deoxygenated by freeze–vacuum–thaw cycles.

**Supported Metal-Cluster Carbonyls.** The alumina pillared clay (0.50 g) was vacuum-dried at 25 °C for 4 h. Under these condtions the clay retains 4.5 wt % water, as indicated by the additional weight loss that occurs under vaccuum at 350 °C. The appropriate metal carbonyl complex (0.02 mmol) in 40 mL of $CH_2Cl_2$ was added under an argon atmosphere to the vacuum-dried clay. The mixture was allowed to stir for 20 h, transferred to a $N_2$-filled glovebox, filtered, washed with $CH_2Cl_2$ to remove unreacted metal carbonyl, and dried under a stream of argon.

**Fischer–Tropsch Reactions.** A stainless-steel tube reactor ($^3/_8$ in.) was operated in the differential mode (<2% conversion) for characterization of Ru–APM catalysts. The reactor tube was fitted with a quartz liner and a quartz frit to contain the catalyst. All reactant gases were ultrahigh-purity grade (Matheson). The gases were further purified by passing them through a manganese/silica adsorbent[33] to remove oxygen, Linde 4A molecular sieves to remove water, and an $Al_2O_3$ adsorbent at −72 °C to remove metal carbonyl contaminants. Products were withdrawn in gaseous form from a heated sample port with a gas-tight syringe or by condensation in a trap cooled to −72 °C. The samples in both gaseous and liquid form were analyzed on a Hewlett-Packard 5890 gas chromatograph fitted with a 0.25 mm × 60 m SPB-1 capillary column with 0.25-$\mu$m film thickness (Supelco) and a flame-ionization detector. Oven temperature programming was utilized to achieve the desired peak separations. Alkane gas mixtures (Scott Specialty Gases) were used for GC calibration. A reference liquid containing $C_7$–$C_{16}$ *n*-alkanes, 1-alkenes, and selected branched hydrocarbons was also used for GC calibration.

Postcatalysis Ru–APM specimens for electron microscopy (STEM) were prepared by dispersing the particles onto holey carbon films mounted on copper grids. The images were obtained on a Vacuum Generators Ltd. HB501 STEM equipped with a field emission gun, annular dark-field detector, and liquid-nitrogen stage.

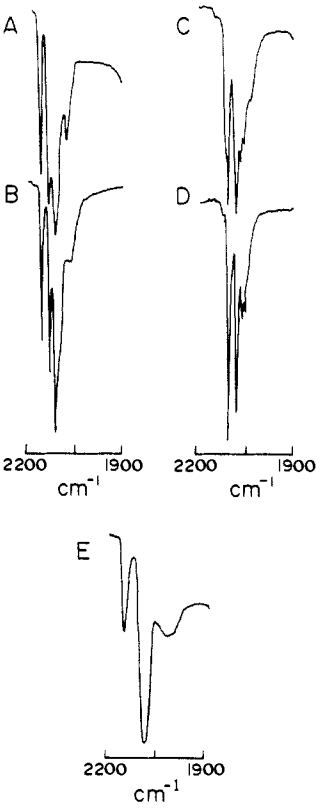


Figure 1. Infrared absorption spectra in the carbonyl-stretching region: (A) $[HOs_3(CO)_{12}^+]$–APM, (B) $[HOs_3(CO)_{12}][PF_6]$, (C) $[Os_3(CO)_{12}]$–APM, (D) $Os_3(CO)_{12}$, (E) $[Os(CO)_x(OAl\equiv)_2]_n$–APM. All samples were prepared as mineral oil mulls, except $Os_3(CO)_{12}$, which was dissolved in $CH_2Cl_2$ solution.

## Results

**$Os_3(CO)_{12}$, $Ru_3(CO)_{12}$, and $Ir_4(CO)_{12}$.** The reaction of $Os_3(CO)_{12}$ in $CH_2Cl_2$ ($5.0 \times 10^{-3}$ M) with APM vaccum-dried at 25 °C results in the binding of a protonated surface cluster (1.0 wt % Os) (eq 1) where the horizontal lines identify the clay-bound

$$Os_3(CO)_{12(soln)} \xrightarrow{APM} \overline{HOs_3(CO)_{12}^+} \qquad (1)$$

species. Parts A and B of Figure 1 compare infrared spectra in the CO-stretching region for the surface-bound cation and an authentic sample of $HOs_3(CO)_{12}^+$ as the $PF_6^-$ salt. The carbonyl-stretching frequencies observed for $HOs_3(CO)_{12}^+$, shown in Table I, are virtually identical with those reported previously.[34]

The clay-bound $HOs_3(CO)_{12}^+$ ions is not desorbed by extensive washing with methylene chloride, as expected for an electrostatic bonding mechanism. However, exposing the dry $[HOs_3(CO)_{12}^+]$–APM to the atmosphere or adding small amounts of water to a $CH_2Cl_2$ suspension causes the cluster to deprotonate, as indicated by the formation of the neutral cluster $Os_3(CO)_{12}$ (cf. parts C and D of Figure 1 and Table I). Thus, the Brønsted acidity of the pillared clay is very dependent on water content (eq 2). The equilibrium indicated in eq 2 can be completely reversed simply by removing the solvent and heating the clay at 100 °C for 2 h.

$$\overline{HOs_3(CO)_{12}^+} + H_2O \rightleftharpoons \overline{H_3O^+ + Os_3(CO)_{12}} \xrightarrow{CH_2Cl_2} \overline{H_3O^+} + Os_3(CO)_{12(soln)} \qquad (2)$$

In further agreement with an electrostatic bonding mechanism for $HOs_3(CO)_{12}^+$, the ion is readily exchanged from the clay surface by $KPF_6$ in acetone (eq 3).

(29) Evans, J.; McNulty, G. S. *J. Chem. Soc., Dalton Trans.* **1984**, 1123.
(30) Deeba, M.; Streusand, B. J.; Schrader, G. L.; Gates, B. C. *J. Catal.* **1981**, *69*, 218.
(31) Pinnavaia, T. J.; Tzou, M. S.; Landau, S. D.; Raythatha, R. H. *J. Mol. Catal.* **1984**, *27*, 195.
(32) Knox, S. A. R.; Koepke, J. W.; Andrews, M. A.; Kaesz, H. D. *J. Am. Chem. Soc.* **1975**, *97*, 3942.
(33) McIlwrick, S. D.; Phillips, C. S. G. *J. Phys. E* **1983**, *6*, 1973.
(34) Knight, J.; Mays, M. J. *J. Chem. Soc. A* **1970**, 711.

$$\overline{HOs_3(CO)_{12}^+} + K^+_{(soln)} \xrightarrow{\text{acetone}} \overline{K^+} + HOs_3(CO)_{12}{}^+_{(soln)} \quad (3)$$

In addition to exhibiting an IR spectrum characteristic of $HOs_3(CO)_{12}^+$, the desorbed cation has λ(max) 366 nm and a hydridic $^1H$ NMR resonance at −19.09 ppm, in agreement with literature values.[34,35] These results show that little or no decarbonylation of the cluster occurs upon protonation in the pillared clay galleries.

Heating the clay-bound $HOs_3(CO)_{12}^+$ ions to 150 °C under vacuum for 2 h causes an irreversible transformation to a new species, with IR properties indicative of ensembles of surface-grafted complexes of the type $[Os(CO)_x(OAl\equiv)_2]_n$ ($x = 2, 3$)[23-25] where OAl≡ represents a surface group on the alumina pillar. The carbonyl absorptions in the infrared spectrum are shown in Figure 1E, and the frequencies are reported in Table I. The same species are formed from $[HOs_3(CO)_{12}^+]$–APM after heating 12 h at 110 °C or after aging 8–10 weeks in air at room temperature. We believe that these species are formed mainly by reaction of the cluster carbonyl with surface hydroxyls of the alumina pillars. Reaction solely at AlOH or SiOH sites at the edges of the host layers is implausible, because only very weak carbonyl absorptions are observed when $Os_3(CO)_{12}$ is allowed to react with the parent montmorillonite under analogous reaction conditions.[36]

The chemistry of $Ru_3(CO)_{12}$ in AMP galleries parallels that described above for the osmium analogue. As is shown by the CO-stretching frequencies listed in Table I, $HRu_3(CO)_{12}^+$ and $Ru_3(CO)_{12}$ can be formed in APM galleries by reactions analogous to those expressed in eq 1 and 2.

The clay-bound protonated cluster is sufficiently stable to the exchanged by $KPF_6$, and the neutral cluster can be desorbed by $CH_2Cl_2$. However, ruthenium species have a much greater tendency to form grafted $[Ru(CO)_x(OA\equiv)_2]_n$ complexes than the corresponding osmium analogues.[28-30] For instance, complete conversion of $[HRu_3(CO)_{12}^+]$–APM to mononuclear $[Ru(CO)_x(OA\equiv)_2]_n$ ensembles occurs within 24 h at 25 °C (cf. Table I), whereas the analogous reaction for the osmium complex requires ~10 weeks. Converting the clay-bound protonated cluster to the neutral cluster by exposure to moist air does not substantially impede formation of the mononuclear ensembles. The greater reactivity of these ruthenium complexes relative to the osmium analogues is consistent with previously observed reactivity patterns on bulk oxides.[24-30]

The interaction of $Ir_4(CO)_{12}$ with APM results in the physical adsorption of the neutral carbonyl (cf. Table I). There is no infrared evidence for protonation or chemical reaction even upon refluxing in cyclohexane. However, $Ir_4(CO)_{12}$ does react at 110 °C to form gallery species with CO-stetching frequencies indicative of $[Ir(CO)_2(OAl\equiv)]_n$ complexes.[27]

**$H_2Os_3(CO)_{10}$ and $H_4Ru_4(CO)_{12}$.** In the absence of air, $H_2Os_3(CO)_{10}$ in $CH_2Cl_2$ solution reacts readily with APM at room temperature to form a surface complex with CO-stretching frequencies characteristic of the grafted cluster species $HOs_3(CO)_{10}(OAl\equiv)$. The CO frequencies (cf. Table I) and relative band intensities are virtually identical with analogous osmium-cluster complexes grafted to the surfaces of bulk alumina and silica.[25-27] Allowing the grafted cluster to age for a few hours in air at 25 °C, or in the absence of air at 150 °C, results in the formation of surface-coupled mononuclear ensembles of $[Os(CO)_x(OAl\equiv)_n$, identical with those formed form the reaction of $Os_3(CO)_{12}$ and APM (cf. Table I). As expected for surface-grafted complexes, neither $HOs_3(CO)_{10}(OAl\equiv)$ nor $[Os(CO)_x(OAl\equiv)_2]_n$ can be desorbed by extensive washing with solvent or by treatment with $KPF_6$ in acetone.

$H_4Ru_4(CO)_{12}$ in $CH_2Cl_2$ adsorbs into the galleries of APM at room temperature by a physical adsorption mechanism, as indicated by the CO-stretching frequencies of the surface-bound complex (cf. Table I). The physisorbed cluster is stable indefinitely at 25 °C in the presence or absence of air, in marked difference from the reactivity of physisorbed $Ru_3(CO)_{12}$ molecules. However, heating $[H_4Ru_4(CO)_{12}]$–APM to 110 °C in air or to 150 °C in vacuo converts the cluster to surface-coupled $[Ru(CO)_x(OAl\equiv)_2]_n$, a species identical with that formed from $Ru_3(CO)_{12}$ (cf. Table I). Among the three CO bands observed for these species, the band near 2140 $cm^{-1}$ most likely is associated with the complex with $x = 3$, because this band decreases with increasing reaction time and the extent of decarbonylation.

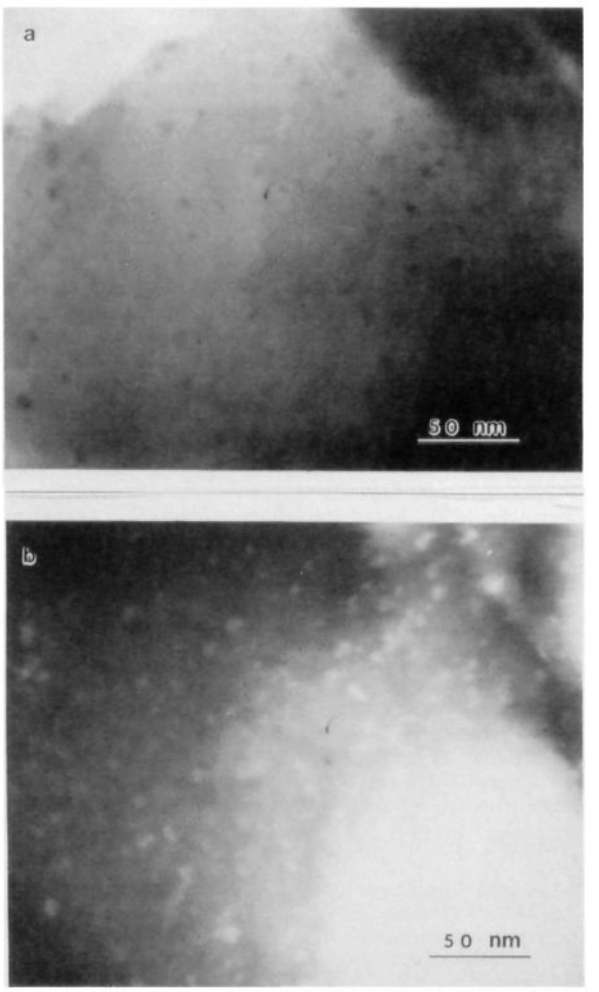


**Figure 2.** STEM images of typical Ru–APM particles after use as a Fischer–Tropsch catalyst: (A) bright field, (B) dark field. Magnification is 500000×.

**Fischer–Tropsch Catalysis.** In view of the unique intracrystalline environment occupied by the metal centers in our pillared clay complexes, we decided to investigate the catalytic properties of $[HRu_3(CO)_{12}^+]$–APM for FT hydrocarbon synthesis. The intercalated cluster was reduced to ruthenium metal in hydrogen under 1 atm pressure at 400 °C for 2.0 h and subsequently exposed to a 2/1 $H_2/CO$ stream at 275 °C (190 psi) for FT catalysis. Conversions in all cases were <2%.

Scanning transmission electron microscopy studies of the Ru–APM clay before and after catalysis indicated the presence of metal aggregates encapsulated *within* the clay support. Figure 2 shows a bright-field STEM image of a typical particle after use as a FT catalyst for 30 h at 275 °C. The vast majority of the observable ruthenium is contained within the clay support with only an occasional metal aggregate appearing at an external surface. Detailed energy-dispersive X-ray analysis, microdiffraction, and *Z*-contrast imaging studies, which have been recently reported elsewhere,[37] demonstrate the presence of pure ruthenium microcrystallites embedded within the pillared clay particles.

(35) Delley, B.; Manning, M. C.; Ellis, D. E.; Berkowitz, J.; Trogler, N. C. *Inorg. Chem.* **1982**, *21*, 2247.
(36) Giannelis, E. P.; Pinnavaia, T. J. *Inorg. Chem.* **1985**, *24*, 2115.
(37) Rightor, E. G.; Pinnavaia, T. J. *Ultramicroscopy* **1987**, *22*, 159.

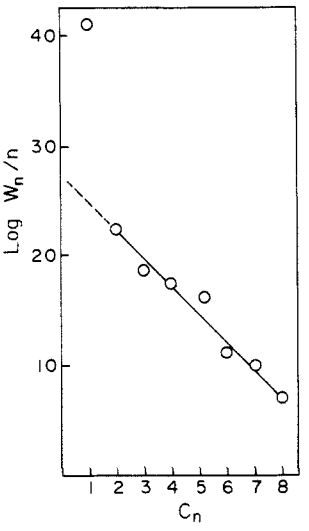


**Figure 3.** Anderson–Schutz–Flory plot of the gaseous hydrocarbons obtained from the reaction of $H_2$ and CO over Ru–APM. Reaction conditions were as follows: 190 psi; $H_2/CO = 2.0$; gas hourly space velocity 2925 $h^{-1}$; 142-min time on stream.

**Table II.** Isomerization to Normal Fischer–Tropsch Hydrocarbon Ratios (I/N) for Ru–APM Catalyst[a]

| carbon no. | I/N | carbon no. | I/N |
|---|---|---|---|
| 4 | 1.79 | 8 | 6.94 |
| 5 | 5.32 | 9 | 2.98 |
| 6 | 6.81 | 10 | 2.22 |
| 7 | 9.75 | 11 | 2.41 |

[a] Reaction conditions were as follows: 275 °C (190 ps); $H_2/CO = 2$; gas hourly space velocity 2930 $h^{-1}$. Ratios were determined after 142-min time on stream.

Figure 3 presents the carbon number distribution of hydrocarbons produced over Ru–APM at 275 °C (190 psi). The results are plotted according to the Anderson–Schulz–Flory expression (eq 4) for chain propagation,[38,39] where $W_n$ is the weight fraction

$$\log W_n/n = n \log \alpha + \log [(1 - \alpha)^2/\alpha] \qquad (4)$$

of hydrocarbon formed with carbon number $n$ and $\alpha$ is the chain-propagation probability. With the exception of methane, the hydrocarbon distribution up to $n = 8$ follows Anderson–Schulz–Flory statistics. Although products are formed with $n \geq 9$, they were not included in the analysis, because of uncertainties in determining their low concentrations at the low conversions (<2%) utilized in this study. The high methane production over Ru results in part from hydrogenolysis of heavier products, as well as from direct methanation.[40] The value of $\alpha$, obtained from the best least-squares fit of the product distribution for $n = 2$–8, is 0.50 ± 0.02.

The most impressive feature of the FT product distribution is the remarkable preference that the catalyst exhibits toward branched products. Ordinarily, Ru supported on bulk oxides provides almost exclusively linear paraffins and linear terminal olefins.[41-48] The linear hydrocarbons are normal FT products,

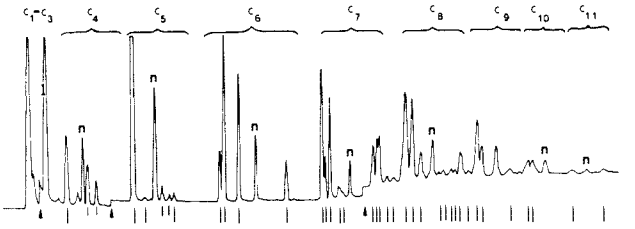


**Figure 4.** Gas chromatogram of Fischer–Tropsch products obtained with Ru–APM as catalyst. Reaction conditions were the same as those described for Figure 3. Peaks labeled *n* are normal-chain paraffins; those labeled with long and short bars are branched-chain products and internal olefins, respectively. Note that internal olefin formation is substantial only for $C_4$ and $C_5$ products. Triangles indicate that times at which the detector gain was increased.

whereas branched hydrocarbons and internal olefins represent isomerized products.

The tendency toward chain branching and internal olefin formation can be qualitatively judged from the gas chromatogram illustrated in Figure 4. The peaks labeled by long and short vertical lines identify the isomerized FT products. Table II provides a quantitative summary of the isomeric to normal FT product ratios (I/N). It is especially significant that the yields of isomerized products are 1.8–9.8 times as large as the normal hydrocarbon yields.

To identify the pathway for chain branching and internal olefin formation, we examined the reactions of known hydrocarbon mixtures over Ru–APM at temperatures similar to those used in the FT studies, except that CO was omitted from the reaction mixture to eliminate chain propagation. When a mixture of ethylene, propylene, and terminal $C_4$–$C_6$ olefins in helium was allowed to react over Ru–APM at 275 °C (olefin/$H_2$ = 1.3–2.8), the principal reactions were hydrogenation and hydrogenolysis, as expected in the absence of CO.[49] However, a substantial fraction of the remaining $C_4$–$C_6$ hydrocarbons was present as internal olefins (20–50%) and branched-chain products (~5%). This latter result suggests that olefin isomerization and branching were important side reactions.

In order to obtain more direct evidence for olefin isomerization and to circumvent the complications caused by hydrogenolysis and hydrogenation, the same olefin mixture described above was allowed to react at 275 °C with the pristine AMP support in the *absence* of dispersed ruthenium. Significanly, the terminal $C_4$–$C_6$ olefins were transformed almost exclusively to internal olefins (~90%) and some branched-chain olefins (~10%). In contrast, no isomerization was observed for $C_4$–$C_6$ *paraffins* under analogous reaction conditions. We conclude, therefore, that the acid-catalyzed isomerization reactions of terminal olefins are the most likely routes to internal olefins and branched-chain products under Fischer–Tropsch conditions.

## Discussion

Our results demonstrate that electrostatically bound, protonated trinuclear clusters of the type $HM_3(CO)_{12}^+$ are the initial products formed by the reaction of $Os_3(CO)_{12}$ and $Ru_3(CO)_{12}$ in the galleries of APM. The Brønsted acidity of the clay is believed to result from the partial thermal dehydration and dehydroxylation of the intercalated polyoxo cations.[50-53] The overall interlayer reaction may be represented qualitatively by eq 5.

$$\underline{Al_{13}O_4(OH)_{24+n}(H_2O)_{12-n}^{(7-n)+}} \xrightarrow{-H_2O} \underline{Al_2O_3{\cdot}xH_2O} + H^+ \qquad (5)$$

(38) Anderson, P. B. In *Catalysis*; Emmett, P. H., Ed.; Reinhold: New York, 1956; pp 345–367.
(39) Madon, R. J. *J. Catal.* **1979**, *57*, 183.
(40) Schulz, H. *C, Mol. Chem.* **1985**, *1*, 231.
(41) Kellner, C. S.; Bell, A. T. *J. Catal.* **1981**, *70*, 418.
(42) King, D. L. *J. Catal.* **1978**, *51*, 386.
(43) Anderson, R. B. *The Fischer–Tropsch Synthesis*; Academic: New York, 1984.
(44) Okuhara, T.; Kumura, T.; Kobayashi, K.; Misono, M.; Yoneda, Y. *Bull. Chem. Soc. Jpn.* **1984**, *57*, 938.
(45) Okuhara, T.; Tamura, H.; Misono, M. *J. Catal.* **1985**, *95*, 41.
(46) Wilson, P.; Bell, A. T. *J. Catal.* **1985**, *17*, 47.
(47) Chuang, S. C.; Tian, Y. H.; Goodwin, J. G., Jr.; Wender, I. *J. Catal.* **1985**, *96*, 396.
(48) Kellner, C. S.; Bell, A. T. *J. Catal.* **1982**, *75*, 251.
(49) Dry, M. E. *Ind. Eng. Chem. Prod. Res. Dev.* **1976**, *15*, 282.
(50) Occelli, M. L.; Tindwa, R. M. *Clays Clay Miner.* **1983**, *31*, 22.
(51) Shabtai, J.; Massoth, F. E.; Tokarz, M.; Tsai, G. M.; McCauley, J. *Proc. 8th International Congress Catalysis*, Verlag Chemie: Berlin, 1984; Vol. IV, p 735.
(52) Plee, D.; Schutz, A.; Poncelet, G.; Fripiat, J. J. *Stud. Surf. Sci. Catal.* **1985**, *20*, 343.
(53) Tichit, D.; Fajula, F.; Figureras, F. *Stud. Surf. Sci. Catal.* **1985**, *20*, 351.

Magic angle spinning NMR studies[54-56] of dehydrated pillared clays indicate that the alumina aggregate is structurally related to the initial polyoxo cation insofar as aluminum is in both octahedral and tetrahedral coordinations. On the basis of the temperature of dehydration and the nature of the host clay, pillar-layer coupling may or may not involve reorganization of the silicate sheet. For montmorillonite, the clay used in the present work, the interaction of the alumina pillar with the clay layers does not lead to structural rearrangement of the tetrahedral sheet at temperatures below 500 °C. Also, the acidic protons are believed to be associated with the hydroxyl groups in the clay layers rather than with basic sites on the pillar.[56]

Lewis acidity, as well as Brønsted acidity, has been postulated to account for the activity of alumina pillared clays as petroleum-cracking catalysts at 500 °C.[57] Evidence for Lewis acid sites, which are believed to arise from coordinatively unsaturated centers on the pillar, has been provided by IR studies of pyridine adsorption.[50,53] Although metal-cluster carbonyls are known to react with strong Lewis acids such as $AlBr_3$,[58] we did not observe adduct formation between $M_3(CO)_{12}$ clusters and APM. Only Brønsted acidity is manifested in our results for $M_3(CO)_{12}$. The strength of the APM as a solid acid is comparable to trifluoroacetic acid or 98% sulfuric acid, the two acids normally needed to protonate $M_3(CO)_{12}$ clusters.[34,35] However, it must be emphasized that the Brønsted acidity of APM depends greatly on the water content. The conversion of gallery $HM_3(CO)_{12}^+$ ions to physisorbed $M_3(CO)_{12}$ species upon the addition of excess water (cf. eq 2) demonstrates the leveling effect of physisorbed water on the gallery acidity.

$Ir_4(CO)_{12}$, $H_2Os_3(CO)_{10}$, and $H_4Ru_4(CO)_{12}$ bind initially in APM galleries by a physical adsorption mechanism. $Ir_4(CO)_{12}$ and $H_2Os_3(CO)_{10}$ are known to exhibit high-field $^1H$ NMR lines upon treatment wtih strong acids, but salts of these protonated species have not been isolated.[34,59] We find no evidence for protonation of these clusters in APM galleries.

The reaction of protonated or neutral metal-cluster carbonyls with the hydroxyl groups of the pillars leads to the degradation of the cluster and formation of oxidized metal carbonyl species grafted to the support. In this regard the pillars exhibit the same surface-reactivity patterns as bulk oxides. For the reaction of $H_2Os_3(CO)_{10}$, a trinuclear $HOs_3(CO)_{10}(OAl\equiv)$ cluster is first grafted to the pillar. An analogous surface species forms from $H_2Os_3(CO)_{10}$ or $Os_3(CO)_{12}$ on bulk silica and alumina.[24-26]

There are three important observations that provide evidence that the surface chemistry observed for metal-cluster carbonyls in APM is occurring in the gallery region of the pillared clay rather than at external surfaces: (i) only trace amounts of $M_3(CO)_{12}$ physisorb to the external surfaces of sodium montmorillonite under comparable conditions where the gallery region is collapsed. (ii) A "stuffed" alumina clay,[60] wherein the pillaring aggregates are so closely spaced that the galleries are not accessible, does not bind $M_3(CO)_{12}$. (iii) the grafting of $[M(CO)_x(OAl\equiv)_2]_n$ ensembles to the external surface silanol groups of montmorillonite requires reaction conditions[36] that are more stringent (~150 °C) than those needed to graft the same clusters to APM (25–110 °C). The first two observations show that the binding capacities toward $M_3(CO)_{12}$ complexes are correlated directly with the *intracrystalline* surface area of the host clay. The third observation indicates that the Al–OH groups of the pillaring alumina aggregate are more reactive than the edge surface silanols of the host layers.

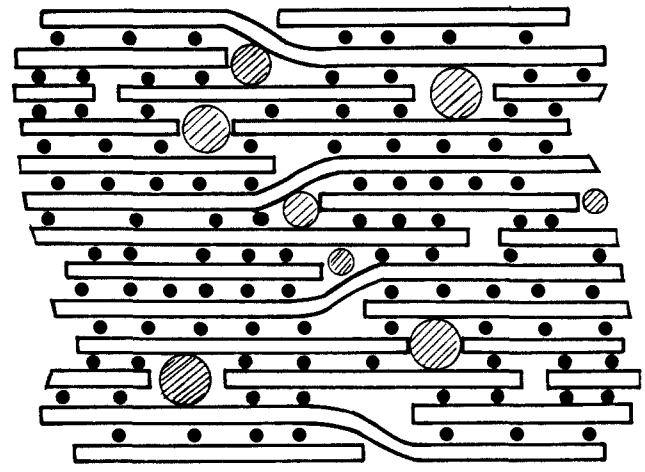

Figure 5. Schematic illustration of suggested defect sites occupied by ruthenium in Ru–APM. Small spheres represent pillaring alumina aggregates between clay layers. Shaded particles represent ruthenium aggregates.

Our results also demonstrate that $[HRu_3(CO)_{12}^+]$–APM is an effective precursor for the dispersion of ruthenium aggregates in the intracrystal environments of the clay host. As a FT catalyst, Ru–APM produces hydrocarbons in accord with the carbon number distributions expected for Anderson–Schulz–Flory chain-propagation statistics (cf. Figure 3). However, the high yields of branched-hydrocarbon products are very atypical of a metal oxide supported ruthenium FT catalyst (cf, Figure 4 and Table II). In this regard the alumina pillared clay behaves very differently from bulk alumina. Normally, straight-chain terminal olefins and the corresponding paraffin hydrogenation products are the major species produced by a ruthenium FT catalyst supported on alumina and other oxides.[41-48]

We propose that the high fraction of branched isomers arises from the protonation of terminal olefins formed by FT chain propagation and the subsequent rearrangement of the carbonium ions[61] on the gallery surfaces. Previous studies of carbonium ion rearrangements on acidic surfaces[62,63] suggest that chain branching most likely occurs via the formation of protonated cyclopropane intermediates (eq 6). The acidity of the APM support is dem-

$$CH_3C^+HCH_2CH_2R \longrightarrow CH_3CH\underset{H^+}{\overset{HCR}{\triangle}}CH_2 \longrightarrow CH_3\underset{CH_3}{CH}C^+HR \quad (6)$$

onstrated by the conversion of terminal olefins to internal olefins and branched-chain hydrocarbons. However, important quantitative differences in the extent of chain branching are observed between the FT products and the products formed by direct olefin isomerization over APM.

For FT products produced at 275 °C, branched-chain products predominate over internal olefins; in fact, branching dominates for all products with carbon numbers greater than $n = 4$. In contrast, the direct isomerization of $C_4$–$C_6$ terminal olefins over pristine APM under equivalent reaction conditions yields mainly linear internal olefins (~90%) and minor amounts of branched products. We attribute these differences to differences in water content and Brønsted acidity. At low FT conversions, the water formed as a by-product most likely chemisorbs to coordinatively unsaturated sites on the pillar. Although excess *physisorbed* water lowers Brønsted acidity (cf. eq 2), *chemisorbed* water at low concentrations can enhance Brønsted acidity through polarization of coordinated molecule (eq 7). Conversely, under the reaction conditions utilized for direct terminal olefin isomerization, little or no chemisorbed water is present to enhance Brønsted acidity.

(54) Plee, D.; Borg, F.; Gatineau, L.; Fripiat, J. J. *J. Am. Chem. Soc.* **1985**, *107*, 2362.
(55) Pinnavaia, T. J.; Landau, S. D.; Tzou, M.-S.; Johnson, I. D. *J. Am. Chem. Soc.* **1985**, *107*, 7222.
(56) Tennakoon, D. T. B.; Jones, W.; Thomas, J. M. *J. Chem. Soc., Faraday Trans. 1* **1986**, *82*, 3081.
(57) Occelli, M. L. *Ind. Eng. Chem. Prod. Res. Dev.* **1983**, *22*, 553.
(58) Kristoff, J. S.; Shriver, D. F. *Inorg. Chem.* **1974**, *13*, 499.
(59) Bryan, E. G.; Jackson, G.; Johnson, B. F. G.; Kelland, J. W.; Lewis, J.; Schorp, K. T. *J. Organomet. Chem.* **1976**, *108*, 385.
(60) Stuffed alumina pillared clays can be obtained by reaction of $Al_{13}$ oligocations with clays of high charge density (e.g. fluorhectorite, vermiculite): Pinnavaia, T. J.; Landau, S. D., unpublished results.
(61) Kramer, G. M.; McVicker, G. B.; Ziemiak, J. J. *J. Catal.* **1985**, *92*, 355.
(62) Gates, B. C.; Katzer, J. R.; Schuit, G. C. A. *Chemistry of Catalytic Process*; McGraw Hill: New York, 1979; pp 20–29.
(63) Weitkamp, J. *Ind. Eng. Chem. Prod. Res. Dev.* **1982**, *21*, 549.

$$\overline{\text{AlOH}_2} \rightarrow \overline{\text{AlOH}^- + \text{H}^+} \quad (7)$$

Evidence for intracrystalline chain propagation is provided by the abundance of 10–50-Å ruthenium aggregates buried within the support particle and the rare occurrence of metal particles on external surfaces (cf. Figure 2). We believe the metal aggregates observed by electron microscopy are formed by migration of ruthenium atoms to defect sites in the clay particle. These defect sites may be formed by layer folding and the formation of interfaces between discrete clay layers, as illustrated in Figure 5, The presence of additional ruthenium, encapsulated within the galleries and too small (<10 Å) to be observed in our electron microscopy studies, is unlikely, Our preliminary $H_2$ chemisorption studies indicate that the Ru dispersion is <10%, as expected for 10–50-Å particles located in defect sites. Even with all the ruthenium contained as larger aggregates in defect sites, the terminal olefins formed by FT chain propagation would still be obliged to contact the highly acidic gallery surfaces in diffusing out of the particle,

Ruthenium as a FT catalyst has been supported on a number of different zeolties.[64-68] In most cases the hydrocarbon products are terminal olefins and normal paraffins. A notable exception is the hydrogen-exchange form of dealuminated zeolite Y, This highly acidic microporous support also affords high yields of isomerized FT hydrocarbons,[67,68] comparable to those observed here for Ru–APM, When ruthenium is introduced into the zeolite by ion exchange and subsequently reduced under hydrogen, metal aggregates as large as 20 Å are embedded within the crystals.[69,70] Thus, there are strong parallels between our alumina pillared clay and hydrogen-exchanged zeolite Y with regard to their intrinsic acidity and ability to support metal particles in intracrystalline environments.

Finally, we note that the high branching selectivity in the FT synthesis of hydrocarbons can have important practical advantages. For instance, the presence of branched isomers in the gasoline range ($C_5$–$C_{12}$) should provide high octane numbers. Also, branching should improve the viscosities of the higher molecular weight fractions used for diesel fuel and jet fuel and as lubricants, Thus, pillared clays are promising materials for the design of selective syn gas catalysts for future energy needs.

**Acknowledgment.** The support of this research by the National Science Foundation, Division of Materials Research (Grant DMR-8514154), and the Michigan State University Center for Fundamental Materials Research is gratefully acknowledged, Fellowship support for E,P,G. and E.G.R. was provided by Exxon Corp, and ICC International, respectively. We thank Dr. Michael Siskin (Exxon) and Dr, Paul Reid (ECC) for their support and helpful discussions.

**Registry No.** $Ru_3(CO)_{12}$, 15243-33-1; $Os_3(CO)_{12}$, 15696-40-9; $Ir_3(CO)_{12}$, 18827-81-1; $H_2Os_3(CO)_{12}$, 12560-48-4; $H_4Ru_4(CO)_{12}$, 34438-91-0; Os, 7440-04-2; Ru, 7440-18-8; Ir, 7439-88-5; montmorillonite, 1318-93-0.

(64) Chen, Y. W.; Wang, h. T.; Goodwin, J. G., Jr. *J. Catal.* **1983**, *83*, 415.
(65) Chen, Y. W.; Wang, H. T.; Goodwin, J. G., Jr. *J. Catal.* **1984**, *85*, 499.
(66) Nijs, N. H.; Jacobs, P. A. *J. Catal.* **1980**, *66*, 401.
(67) Tatsumi, T.; Shul, Y. G.; Sugivra, T.; Tominaga, H. *Appl. Catal.* **1986**, *21*, 119.
(68) King, D. L. *J. Catal.* **1978**, *51*, 386.
(69) Verdonck, J. J.; Jacobs, P. A.; Gent, M.; Poncelet, G. *J. Chem. Soc., Faraday Trans. 1* **1980**, *76*, 403.
(70) Gustafson, B. L.; Lunsford, J. H. *J. Catal.* **1982**, *74*, 393.

# The Influence of Guest–Host Interactions on the Excited-State Properties of Dioxorhenium(V) Ions in Intracrystalline Environments of Complex-Layered Oxides

**Mark D. Newsham, Emmanuel P. Giannelis, Thomas J. Pinnavaia,* and Daniel G. Nocera***

*Contribution from the Department of Chemistry and the Center for Fundamental Materials Research, Michigan State University, East Lansing, Michigan 48824-1322.*
*Received October 16, 1987*

**Abstract:** The excited-state properties of *trans*-dioxorhenium(V) ions immobilized in the intracrystalline environments of three complex-layered oxides (CLOs) have been examined. The layered silicate CLOs hectorite and fluorohectorite adsorb *trans*-$ReO_2(py)_4^+$ to their negatively charged interlayers by intercalative ion exchange to produce topotactic solids with gallery heights of 6.7 and 9.2 Å, respectively. A dioxorhenium CLO of complementary charge, prepared by the addition of NaOH to an aqueous solution containing $MgCl_2$:$AlCl_3$ (1:2 w/w) and *trans*-$ReO_2(CN)_4^{3-}$, incorporates the oxoanion between the positive layers of a hydrotalcite-like Mg/Al double hydroxide. Electronic absorption and vibrational spectra of these three CLO intercalates are characteristic of the dioxorhenium ions and are indicative of structurally unperturbed oxo complexes in the CLO intracrystalline environment. Despite structurally similar intercalated *trans*-$ReO_2^+$ cores, steady-state and time-resolved luminescence experiments reveal that the three CLO intercalates are quite distinct: solid $ReO_2(py)_4$–hectorite is highly emissive ($\lambda_{em,max}$ = 630 nm at 25 °C) and luminescence spectra display progressions in 900-$cm^{-1}$ ($\nu_{a_{1g}}$(Re–O)) and 200-$cm^{-1}$ ($\nu_{a_{1g}}$(Re–py)) modes similar to that of the native ion; $ReO_2(py)_4$–fluorohectorite exhibits broad and featureless emission ($\lambda_{em,max}$ = 685 nm at 25 °C) whose intensity is attenuated by a factor of 50 relative to the hectorite compound and, $ReO_2(CN)_4$–hydrotalcite does not luminesce. The luminescence decay curve of $ReO_2(py)_4$–hectorite displays multiexponential form with a major lifetime component of 13.0 μs and a minor lifetime component of 3.9 μs. In contrast, the emission decay of the fluorohectorite intercalate is uniexponential and fast ($\tau$ = 0.63 μs). The disparate excited-state properties of the three intercalates are attributed to specific guest–host interactions which mediate the reaction between the *trans*-$ReO_2^+$ core and water in the CLO interlayers.

Photochemical processes can significantly be modified with the intercalation of reactants within intracrystalline environments of zeolites,[1-4] layered phosphates,[5] and complex-layered oxides (CLOs).[6-10] Layered silicate clays (LSCs) and layered double

0002-7863/88/1510-3885$01.50/0 